Characterization of anisotropic poly(vinyl alcohol) hydrogel by small- and ultra-small-angle neutron scattering. J Chem Phys 130:034903

6 AUTHORS, INCLUDING:

Mu-Ping Nieh
University of Connecticut
107 PUBLICATIONS **1,808** CITATIONS

SEE PROFILE

J. Pencer
Canadian Nuclear Laboratories
57 PUBLICATIONS **1,028** CITATIONS

SEE PROFILE

Characterization of anisotropic poly(vinyl alcohol) hydrogel by small- and ultra-small-angle neutron scattering

Stephen D. Hudson,[1] Jeffrey L. Hutter,[1,a)] Mu-Ping Nieh,[2,b)] Jeremy Pencer,[2] Leonardo E. Millon,[3] and Wankei Wan[3]

[1]*Department of Physics and Astronomy, The University of Western Ontario, London, Ontario N6A 3K7, Canada*
[2]*Canadian Neutron Beam Centre, National Research Council Canada, Chalk River, Ontario K0J 1J0, Canada*
[3]*Department of Chemical and Biochemical Engineering, The University of Western Ontario, London, Ontario N6A 5B9, Canada*

Poly(vinyl alcohol) (PVA) hydrogels are formed from PVA solution when physical cross-links form during freeze/thaw cycling. By applying a stress during the freeze/thaw process, PVA hydrogels with anisotropic mechanical properties are produced. We have used small- and ultra-small-angle neutron scattering to study the structure at length scales of 2 nm to 10 μm. By supplementing the neutron data with data from atomic force microscopy, we have probed a large range of length scales within which structural changes responsible for bulk anisotropy occur. We model the gel as interconnected PVA blobs of size 20–50 nm arranged in fractal aggregates extending to micrometers or tens of micrometers. Bulk mechanical anisotropy appears to be due to the alignment of blobs and connections between blobs. This information is essential for tailoring mechanical properties for applications where anisotropy is desirable such as to match the properties of natural tissue in coronary grafts and to control diffusive properties in active wound dressings. © *2009 American Institute of Physics.* [DOI: 10.1063/1.3050096]

I. INTRODUCTION

Poly(vinyl alcohol) (PVA) hydrogel is a hydrophilic, biocompatible material that has received recent attention for a variety of applications. For instance, physically cross-linked PVA hydrogels can be tailored to have mechanical properties similar to those of cardiovascular tissue,[1–5] raising the possibility of its use in cardiovascular prostheses with a reduced risk of failure due to compliance mismatch.[6,7]

Physically cross-linked PVA hydrogels are formed from PVA solution during freeze/thaw thermal cycling or quenching. The mechanism by which PVA solution gels during thermal cycling has received much attention.[1,3,8–10] The generally accepted model is that cycling to low temperatures causes the formation of ice crystals, which increases the polymer concentration in the surrounding, unfrozen regions, inducing PVA crystallization. Using solid-state nuclear magnetic resonance, differential scanning calorimetry, and small-angle x-ray scattering, Willcox *et al.*[10] showed that PVA crystallites of size 3–8 nm and average separation of 30 nm form in the concentrated polymer regions. Cryogenic transmission electron microscopy showed that the dense, crystallite-filled regions surround much larger ice crystals where little polymer is found.

Recently, an anisotropic PVA hydrogel has been reported, in which anisotropy is induced by stretching a weak isotropic gel formed by a single thermal cycle, followed by further cycling.[4] The authors were able to optimize the stress-strain properties of the anisotropic PVA hydrogel to match those of porcine aorta in the physiological range, raising the possibility of use for cardiovascular tissue replacement. Small-angle neutron scattering (SANS) studies of this anisotropic hydrogel showed that its anisotropic properties were due to structural changes at a scale larger than 100 nm.[5]

In this study we use ultra-SANS (USANS) to extend the length scale probed to approximately 10 μm and measure a wide range of gels formed by varying the number of thermal cycles and the amount of processing strain. Here we present a combined SANS and USANS study of thermally cycled anisotropic PVA hydrogels.

II. MATERIALS AND METHODS

A. Sample preparation

PVA solutions were prepared by dissolving atactic PVA with an average molecular weight of 146 000–186 000 (99+% hydrolyzed, Sigma-Aldrich, Canada) in deuterium oxide (D_2O) (99.9 at. %, Sigma-Aldrich, Canada) to achieve a D_2O:PVA molar ratio of 21.9:1, closely matching the molar ratio used in previous studies,[4,5] in which H_2O was the solvent. The solutions were held at 90 °C while stirring for 3 h as reported previously[5] to fully dissolve the PVA. A reflux column and drying tube containing anhydrous calcium sulfate (Drierite, Sigma-Aldrich, Canada) were used to prevent the loss of D_2O and to minimize exchange with H_2O in the air.

The PVA solution was used to fill molds comprised of 17.8×17.8 cm^2 plates of aluminum separated by a 1.6 mm

TABLE I. NG3 SANS configurations.

SDD (m)	λ (Å)	q (Å^{-1})	r (nm)
1.33[a]	6.0	0.033–0.3[b]	2.1–19
5.0[a]	6.0	0.0099–0.11	5.7–63
13.19[ac]	8.4	0.0013–0.031	20–480

[a]Detector offset 20 cm from center to achieve a larger q-range at a particular SDD.
[b]Maximum q limited by sample cell geometry.
[c]Lens configuration to achieve low q.

thick rubber gasket. The solution was carefully added to the molds using a syringe to prevent the introduction of air bubbles. Molds were sealed and submerged in a water bath for thermal cycling. Each cycle consisted of ramping the temperature from 20 to −20 °C at 0.1 °C/min, holding the temperature at −20 °C for 1 h, ramping the temperature back to 20 °C at 0.1 °C/min, and holding the temperature at 20 °C for 1 h. This cycle was repeated as required.

Anisotropic gels were made by stretching cycle 1 gels and securing them in modified aluminum molds with clamps. The extension required for the desired strain was determined before stretching and measured with a ruler during stretching. Each clamp consisted of a thin aluminum strip that could be screwed, through the gel, into the bottom aluminum plate.[5] Further cycling with this setup resulted in gels with *permanent* anisotropic properties.

B. Neutron scattering

SANS experiments were performed on the NG3 beamline at the National Institute of Standards and Technology (NIST) in Gaithersburg, MD.[11] Three sample-to-detector distance (SDD) and wavelength (λ) combinations were used to cover a scattering vector (q) range from 0.0013−0.3 Å^{-1}, as shown in Table I. The corresponding length scales $r=2\pi/q$ range from 2.1 to 480 nm. At large scattering angles of the shortest SDD configuration, the geometry of the titanium sample holders caused a reduction in neutron counts at scattering vectors above a magnitude of 0.3 Å^{-1}. For this reason, data above this scattering vector magnitude were not used. At the longest SDD configuration, a focusing lens system consisting of concave MgF$_2$ lenses was used to provide better low-q resolution and higher flux than could be attained using a conventional pinhole collimation system.[12] Examples of raw data from isotropic and anisotropic gels are shown in Fig. 1.

USANS experiments were performed at NIST on the BT5 instrument, which is an ultrahigh resolution small-angle neutron scattering double-crystal diffractometer.[13] This instrument collects one-dimensional data, so anisotropic samples were run twice: once with the processing strain direction parallel to the scattering plane, and once with the sample rotated in plane by 90°, i.e., with the processing strain direction perpendicular to the scattering plane. Neutrons of wavelength 2.38 Å are selected by Bragg reflection from perfect-crystal monochromators and reflected toward the sample. Behind the sample, an analyzer, also consisting of a perfect-crystal monochromator, is rotated to reflect scat-
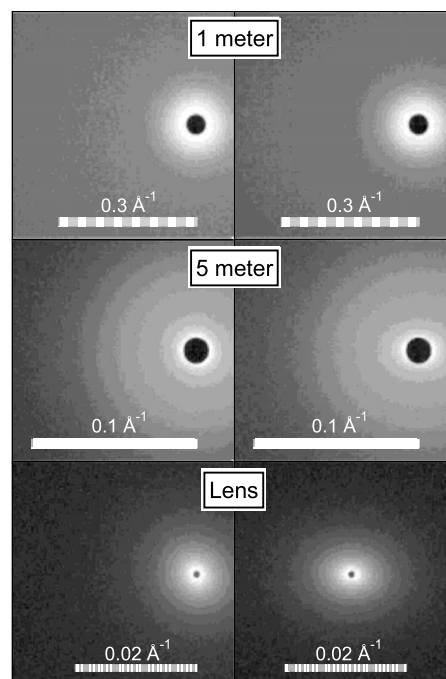

FIG. 1. Raw SANS data for isotropic (left column) and anisotropic (right column) cycle-six PVA hydrogels using the NG3 configurations shown in Table I. The scale bars indicate the scattering vector, q, with the largest q range occurring at the nearest detector position (1 m) and the smallest q range occurring at the farthest detector position (lens, 13 m). The brightness represents the logarithm of the total number of neutrons counted on the detector (arbitrary scale), and is not corrected for background or the contribution of the sample cell. Sixteen gray scale colors have been used in order to show contours of constant neutron counts, elucidating the anisotropy. Note that a beam stop is used to prevent detector damage due to the unscattered beam, resulting in dark spots centered at $q=0$. The strain induced during cycling for the anisotropic gel was 75%, resulting in an anisotropy that is most obvious at the largest length scales (smallest q).

tered neutrons into a detector. Due to the high angular sensitivity of Bragg reflection, only neutrons that are scattered through a very narrow range of angles are diffracted by the analyzer into the detector, providing excellent angular resolution extending to very small angles. By rotating the analyzer to a maximum angle of 0.046°, scattering vectors up to 0.0021 Å^{-1} and length scales down to 300 nm were studied, providing overlap with the SANS data.

Data were collected for hydrogel samples made with various numbers of thermal cycles and processing strains. However, due to time constraints, not all of the samples studied by SANS could be studied with USANS. Table II shows

TABLE II. PVA samples and scattering techniques used.

N	ϵ_0	Scattering techniques
1	0	SANS, USANS
3	0	SANS, USANS
	0.25	SANS
	0.50	SANS
	0.75	SANS, USANS
6	0	SANS, USANS
	0.25	SANS, USANS
	0.50	SANS
	0.75	SANS, USANS

the combinations of thermal cycles, N, processing strains, ϵ_0, and scattering techniques employed. Priority was given to samples produced with a strain of 0.75, as a cycle 3 hydrogel produced with a strain of 0.75 was shown to closely match the stress-strain properties of porcine aorta.[4] Isotropic samples are unstretched and have processing strains of zero. Samples were considered fresh, as they were prepared less than one month before the neutron scattering experiments and we have previously verified that the mechanical properties of anisotropic PVA hydrogels do not change significantly after aging for 13 months.[5]

C. Data reduction

Differential scattering cross sections ($d\Sigma/d\Omega(q)$) were extracted from the SANS data in Igor Pro (WaveMetrics, Inc., Portland, OR) using routines provided by NIST.[14] Briefly, the data were corrected for background and empty sample cell scattering, divided by the sensitivity of the detector, and converted to absolute scaling in units of cm^{-1}. One-dimensional differential scattering cross sections were extracted by circularly averaging the isotropic data about the $q=0$ position. In the case of anisotropic gels, two one-dimensional cross sections were obtained by sector averaging parallel and perpendicular to the direction of applied strain. We chose an angular width of 45° for all sector averages, which showed negligible difference from 30° sector averages. For each sample, data from the three q-ranges were combined into a single SANS data set spanning a range of $0.0013 < q < 0.3$ Å^{-1}.

USANS data were also reduced using Igor Pro routines provided by NIST.[14] Similar to SANS data reduction, this also involved subtraction of background and empty cell scattering and conversion to absolute scaling. In order to facilitate simultaneous fitting to SANS and USANS data, NIST's implementation[14] of the Lake algorithm[15] was used to deconvolve the smearing due to the finite angular range of neutrons outside of the nominal scattering plane. The Lake algorithm uses an iterative algorithm to deduce what the scattering observed using an infinitesimally small pinhole would be, given the smeared scattering observed using a collimation slit of known dimensions. In practice, unscattered neutrons are detected at very low q-values, creating large background and limiting the maximum length scale that can be probed. For a few data points at low q, the empty cell scattering counts outnumber the sample scattering counts. After subtraction and absolute scaling, these points show negative scattered intensity. While desmearing, these low q data points with negative intensities were masked. No data smoothing was used prior to desmearing. After desmearing, the remaining noisy points at low q were eliminated, leaving useable data up to approximately 10 μm.

D. Atomic force microscopy

A PVA hydrogel was studied using a BioScope II atomic force microscope (Veeco Metrology Inc., Santa Barbara, CA). A cycle 10 hydrogel was imaged because it was stiffer than hydrogels made with fewer thermal cycles, thus allowing higher resolution imaging. NP-S silicon nitride cantile-

vers with nominal spring constants of 0.06 N/m (Veeco Metrology Inc., Santa Barbara, CA) were used. Imaging was performed in water with unmodified cantilevers and cantilevers modified by 20 μm glass beads (Duke Scientific Corporation, Palo Alto, CA) glued to their ends with NOA 81 ultraviolet-curing optical adhesive (Norland Products Inc., New Brunswick, NJ). Modified glass bead tips greatly reduced sample damage and imaging artifacts at the expense of imaging resolution, and were reserved for imaging at the largest scan size where imaging resolution was less important.

III. THEORY AND DATA ANALYSIS

Neutron scattering results from variations of the scattering length density in the sample. In PVA hydrogels, there is good contrast between the polymer and solvent, so variation in polymer concentration results in variation in the scattering length density. Our goal is to deduce the polymer concentration as a function of position from the scattered neutrons. However, as with most scattering techniques, only the intensity of the scattered waves is measured while the amplitudes and phases of individual scattered waves are unknown, making it impossible to directly deduce the polymer concentration as a function of position. Instead, one generally hypothesizes a structure and compares the predicted scattering to that observed. Care must be taken because a concentration distribution that gives the measured scattering is not unique.

A. Solution

For PVA with an average molecular weight of 146 000–186 000 g/mol, we calculate that the overlap concentration is roughly 0.6% by mass in a good solvent.[16] At 10% polymer by mass, our PVA solution is well above the overlap concentration but well below 100%. Scattering from a neutral, ungelled polymer solution in this "semidilute" regime is expected to exhibit Ornstein–Zernicke (Lorentzian) behavior described by

$$\left(\frac{d\Sigma}{d\Omega}\right)_{sol}(q) = \frac{A_{sol}}{1 + (q\xi_{sol})^2} + bg, \tag{1}$$

where A_{sol} is a constant incorporating the osmotic compression modulus, the inherent D$_2$O–PVA contrast, and the volume fraction; ξ_{sol} is the density-density correlation or screening length;[16] and bg includes background and incoherent scattering.

A fit of Eq. (1) to the differential scattering cross section of the uncycled solution is shown in Fig. 2 and yields a screening length of 2.9 nm, in agreement with the value of 3 nm expected from a rough approximation in which linear chains are evenly spaced along the directions parallel to each of the three Cartesian axes. Although some gelation will occur without freeze/thaw cycling, Fig. 2 shows good agreement between Eq. (1) and the scattering from our solution.

B. Hydrogel

When the PVA solution is thermally cycled, PVA crystallites form and act as cross-linking sites.[1,8,10] Our model for
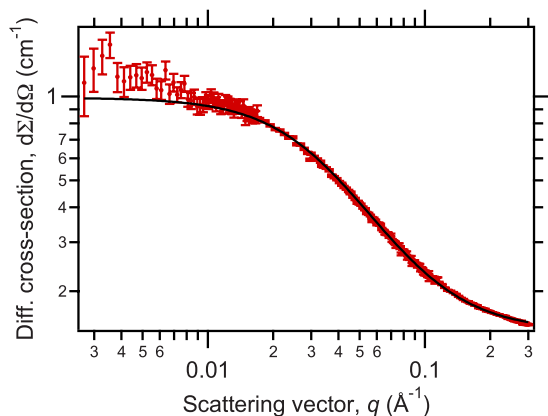
FIG. 2. (Color online) Differential scattering cross section from PVA solution after reduction to an absolute scale and circular averaging. The solid line is the fit to Eq. (1).
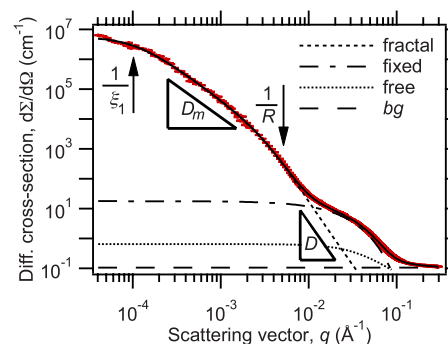

FIG. 3. (Color online) Differential scattering cross section from a cycle 1 PVA hydrogel. The solid line is the model fit to the data, i.e., the sum of the individual scattering terms in Eq. (8). The contributions of individual terms are indicated by dashed lines. Triangles are shown to mark the slopes that determine the mass fractal dimension, D_m, and surface fractal dimension, $d_s = 4 - D/2$. The positions where the slope changes determine the mass fractal aggregate size, ξ_1, and blob size, R.

the hydrogel structure is motivated by previous studies that suggest the crystallites are a few nanometers in size and separated by tens of nanometers.[5,10,17,18]

We model the gel as a combination of polymer that is cross-linked and fixed, and polymer that is free to move.[19–23] This approach has been applied successfully to a variety of chemically cross-linked polymer gels,[19,21,24] including chemically cross-linked PVA[23] (see Ref. 22 for a good review). We refer to this model as the Horkay–Geissler model.

Scattering from the free polymer, e.g., polymer in solution without cross-links, is still described by an Ornstein–Zernicke term and will be referred to as free polymer scattering. Thus

$$\left(\frac{d\Sigma}{d\Omega}\right)_{\text{free}}(q) = \frac{A_{\text{free}}}{1 + (q\xi_{\text{free}})^2}, \tag{2}$$

where A_{free} and ξ_{free} are expected to differ from the corresponding values in the ungelled solution because the PVA density in regions containing free polymer will be different than the density in the initial solution.

Permanent density fluctuations in the cross-linked polymer are assumed to have a Gaussian density correlation function,[19] or more generally,[21] a density correlation of the form

$$\rho(r) \propto \exp[-(r/\xi_{\text{fixed}})^b], \tag{3}$$

where ξ_{fixed} is the average size of the fixed density fluctuations and b is a constant that determines how abruptly the density changes with distance. The Fourier transform of Eq. (3) yields a fixed scattering function of

$$\left(\frac{d\Sigma}{d\Omega}\right)_{\text{fixed}}(q) = A_{\text{fixed}} \exp[-(q\xi_{\text{fixed}})^b], \tag{4}$$

where A_{fixed} depends on the scattering contrast and concentration.

While the Horkay–Geissler model[21] successfully describes our data at high q, we see significant excess scattering at low q (Fig. 3), which we attribute to scattering from large polymer-poor voids where ice crystals have melted. We model the polymer structure surrounding the pores as a net-

work of dense polymer knots or blobs, each of which has an internal structure described by the small-scale gel structure discussed above.

The PVA blobs cannot be considered sparse and noninteracting, so it is necessary to consider interference effects from scattering between the blobs. This is accomplished by modeling the data as the product of a form factor, $P(q)$ that describes the scattering from a single blob, and a structure factor, $S(q)$ that describes the arrangement of all of the blobs and the resulting interference.

The blobs are expected to be irregular and to have a distribution of sizes, but without evidence that indicates what the distribution should be, it is difficult to justify increasing the number of parameters by integrating a basic form factor (e.g., the form factor for a sphere) over a distribution of radii. Instead, we opt to use a form factor similar to the Debye–Anderson–Brumberger form factor

$$P(q) \propto \frac{1}{[1 + (q\xi)^2]^2} \tag{5}$$

that was derived for a randomly distributed phase of correlation length ξ.[25] For nonuniform objects that are approximately spherical, ξ is proportional to the average radius of the objects.[26] However, the low-q contribution to our scattering data does not obey the Porod power law in the high-q limit. For all samples made with three or six thermal cycles, the power-law exponent, which can be determined from the slope on a log-log plot, is shallower than -4, indicating that the interface has a rough or surface fractal structure. We therefore modify the exponent to obtain the form factor[27]

$$P(q) = \frac{A_1}{\left[1 + \dfrac{D+1}{3}(Rq)^2\right]^{D/2}}, \tag{6}$$

where R is the average size of the blobs, D is related to the surface fractal dimension d_s by $D = 2(4 - d_s)$, and A_1 is a scattering amplitude. The surface fractal dimension can vary from 2 for a perfectly smooth surface to 3 for a surface with maximum roughness. For this range of d_s, D can vary between 2 and 4.
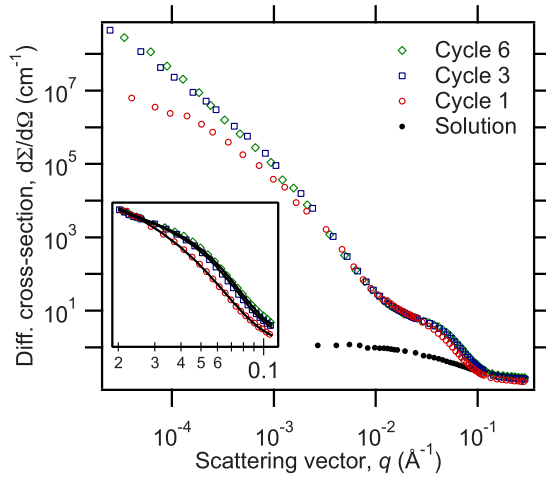
FIG. 4. (Color online) Differential scattering cross sections from cycle 1, 3, and 6 PVA hydrogels. Four-fifths of the data points have been omitted for clarity, and data for solution are included for comparison. Inset: high-q scattering data dominated by the small-scale fixed polymer scattering. The solid lines are the model fit to the data.

The USANS and atomic force microscopy (AFM) data (see below) indicate that structures extend to length scales of at least 10 μm. To capture this behavior, we use the mass fractal structure factor

$$S(q) = 1 + \frac{D_m \Gamma(D_m - 1)}{(qR)^{D_m}} \left[\left(1 + \frac{1}{(q\xi_1)^2} \right)^{(1-D_m)/2} \right.$$
$$\left. \times \sin[(D_m - 1)\arctan(q\xi_1)] \right], \qquad (7)$$

where D_m is the mass fractal dimension, Γ is the gamma function, R is the average blob size from Eq. (6), and ξ_1 is the upper limit of the fractal structure.[28] This allows the scattering to roll off as q decreases to values corresponding to the aggregate size ξ_1.

The complete model for the hydrogel structure is then

$$\frac{d\Sigma}{d\Omega} = P(q)S(q) + \left(\frac{d\Sigma}{d\Omega} \right)_{\text{fixed}} + \left(\frac{d\Sigma}{d\Omega} \right)_{\text{free}} + bg. \qquad (8)$$

The first term is for scattering from the large structure of PVA blobs, the second term describes the density fluctuations
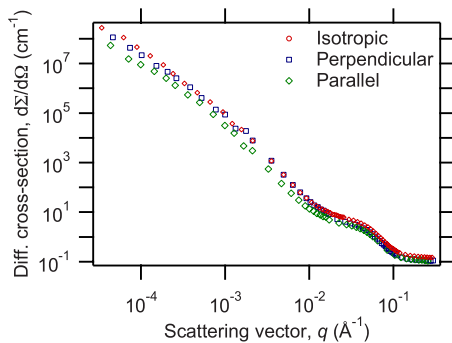

FIG. 5. (Color online) Differential scattering cross sections from cycle 6 PVA hydrogels. Data are shown for an isotropic gel and for an anisotropic gel produced with a processing strain of 75%. The anisotropic data are from sector averages parallel and perpendicular to the direction of the processing strain. Four-fifths of the data points have been omitted for clarity.

TABLE III. Fractal aggregate sizes as determined by fitting Eq. (8) to combined SANS and USANS data. For anisotropic gels, the initial processing strain was 75% unless noted otherwise.

	Aggregate size, ξ_1 (μm)		
Cycle	Isotropic	Perpendicular	Parallel
1	0.9	$\cdots$	$\cdots$
3	~ 10	3.4	>10
6	2.4	2.9[a]	>10[a]
6		4.3	>10

[a]Processing strain of 25%.

in the blobs due to cross-linking of the polymer molecules, and the free scattering term has been included to determine if there is any remaining free polymer (i.e., polymer that has not been cross-linked). Finally, a constant term has been included to account for background and incoherent scattering, giving a total of 11 parameters.

An example fit is shown in Fig. 3, in which the full model of Eq. (8) is shown with a solid line, and the contributions of individual terms are indicated by dashed lines. Figure 3 also shows the slopes that are determined by the mass and surface fractal dimensions, as well as the transitions between slopes that are determined by the fractal aggregate size and the blob size. Figure 4 shows how the neutron data change with the number of thermal cycles and Fig. 5 shows neutron data for an isotropic cycle 6 hydrogel, and an anisotropic cycle 6 hydrogel produced with a processing strain of 75%.

C. Data fitting

The blob size R determines where the transition between the slopes of D_m and D occurs. The overlap between USANS and SANS data occurs at approximately the same magnitude of q as this transition, and neither data are sufficient to determine R alone. For this reason, we performed the fitting in two steps. In the first, ξ_1, D_m, and R are determined by fitting to Eq. (8) for samples in which both SANS and USANS data were acquired. In the second, d_s, ξ_{fixed}, b, ξ_{free}, and bg are determined by fitting Eq. (8), with the larger scale parameters held constant, for samples in which only SANS data were acquired.

Fractal aggregate sizes determined by fitting combined SANS and USANS data sets to the full model of Eq. (8) are shown in Table III. Blob sizes versus number of thermal cycles are shown in Table IV for isotropic and anisotropic gels. While there is a wide variation in parameters, it is clear that for anisotropic gels both R and ξ_1 show a significant difference between the perpendicular and parallel directions. The mass fractal dimension showed no clear trends with the number of thermal cycles or with direction in anisotropic gels and had an average value of 2.2 ± 0.2.

Where supplementary USANS data do not exist, the large-scale structure parameters cannot be determined because the fractal aggregate size is well beyond the range of the SANS data, and the transition between the slopes D_m and D (Fig. 3) occurs approximately at the lower limit of the

TABLE IV. Blob sizes as determined by fitting Eq. (8) to combined SANS and USANS data. For anisotropic gels, the initial processing strain was 75% unless noted otherwise.

Cycle	Blob size, R (nm)		
	Isotropic	Perpendicular	Parallel
1	18	⋯	⋯
3	51	46	76
6	40	27[a]	34[a]
6		29	78

[a]Processing strain of 25%.

SANS data. No clear trend was observed for the mass fractal dimension versus the number of thermal cycles, so we chose to hold D_m constant at the value of 2.2 determined above. For this value of D_m, the structure factor [Eq. (7)] reduces to

$$S(q) = 1 + \frac{1.92}{(qR)^{2.2}} \tag{9}$$

in the limit $q\xi_1 \gg 1$. The smallest product $q\xi_1$ occurs for the cycle 1 gel (smallest ξ_1), and in this case, the full structure factor differs from Eq. (9) by 2.6%. Therefore, for all SANS data, Eq. (9) differs from Eq. (7) by 2.6% or less, justifying the elimination of ξ_1 and the use of Eq. (9) for the structure factor during fitting.

Although R was allowed to vary as a fit parameter, we deemed that the values returned were not reliable except from cycle 1 where R is smallest. Plots of d_s, ξ_{fixed}, and b versus the processing strain ϵ_0 are shown in Figs. 6–8, respectively. ξ_{free} shows no anisotropy and little or no dependence on N and has a mean value of 2.7 ± 0.2 nm.

IV. DISCUSSION

It is well established that PVA hydrogels are cross-linked by polymer crystallites formed during thermal processing. Our modeling of SANS and USANS data and AFM imaging shows that the cross-linked polymer is concentrated into relatively dense blobs with a length scale of a few nanometers assembled in a structure with mass fractal characteristics up to a length scale of at least several micrometers. An-
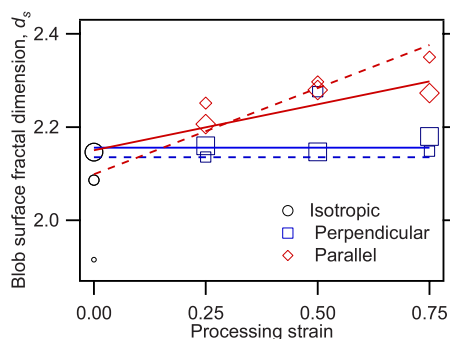

FIG. 6. (Color online) Surface fractal dimension vs processing strain. Data for cycles 1, 3, and 6 are represented by small, medium, and large symbols, respectively. Trends vs processing strain are shown for cycle 3 (dashed lines) and cycle 6 (solid lines). Error bars (not shown for clarity) range from 0.02 to 0.09.
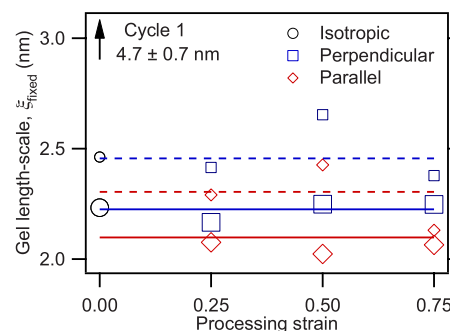

FIG. 7. (Color online) Fixed gel length scale vs processing strain. Data for cycles 1, 3, and 6 are represented by small, medium, and large symbols, respectively. Average values are shown for cycle 3 (dashed lines) and cycle 6 (solid lines). Error bars (not shown for clarity) range from 0.02 to 0.1.

isotropic gels show similar characteristics, but exhibit longer length scales in the direction of the strain applied during processing.

A. Isotropic gels

The smallest length scales (highest q) show a feature that is well modeled by the density correlation function previously applied to cross-linked gels by Horkay and Geissler. The characteristic length of the density fluctuations, 4.7 nm, obtained by a fit to this model for a weak, cycle 1 gel, is larger than the screening length of 2.9 nm obtained for the ungelled solution, but the relative sharpness of the feature (see Fig. 4) and exponential (versus power-law) decay of the correlation function indicates a more compact structure. This argues that the gelation process has concentrated the PVA into clumps, which we take to be crystallites surrounded by dangling chains. This necessarily means that other regions have been depleted of polymer, consistent with the structure of polymer-poor pores that has been previously described.

Continued cycling systematically decreases the length scale ξ_{fixed} of the density fluctuations and sharpens the fall-off of the correlation function parametrized by the exponent b as shown in Figs. 7 and 8 versus processing strain, respectively (the present discussion focuses on a processing strain of 0 only). It is thus apparent that the freeze/thaw process enhances the density fluctuations and expels water from the polymer-rich regions, possibly by increasing the size and perfection of existing crystallites and/or by nucleating addi-
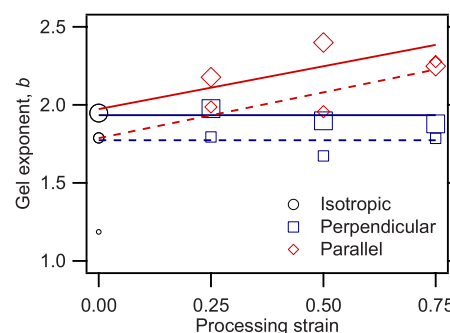

FIG. 8. (Color online) Gel exponent vs processing strain. Data for cycles 1, 3, and 6 are represented by small, medium, and large symbols, respectively. Trends vs processing strain are shown for cycle 3 (dashed lines) and cycle 6 (solid lines). Error bars (not shown for clarity) range from 0.01 to 0.07.
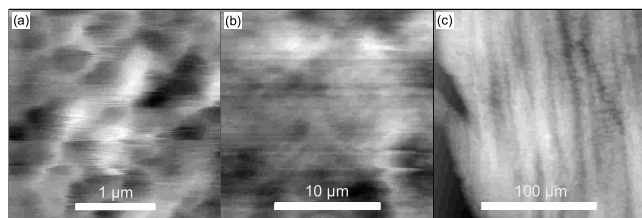
FIG. 9. Contact mode AFM images of a cycle 10 PVA hydrogel that were taken under fluid. Images (a) and (b) were acquired with unmodified tips and image (c) was acquired with a 20 μm glass bead tip.

tional crystallites, as described previously.[29] This indicates that thermal cycles promote separation between water and PVA on nanometer scales.

Larger length scales, represented by q values below 0.01 Å^{-1} in Fig. 4, show that the density fluctuations are organized into large structures. The observation that the scattering data do not level off for small q, except possibly for the weakest gel, indicates features extending from ~ 1 μm for cycle 1 gels to at least several micrometers for cycle 3 and 6 gels. We were not able to successfully model the low-q regime using structures described by a single length scale (e.g., the Debye–Anderson–Brumberger form factor), so we chose to consider a structure of blobs of characteristic size R and surface fractal dimension d_s arranged in a mass fractal aggregate of dimension D_m and extent ξ_1.

Our modeling reveals that the blob size increases abruptly from 18 to ~ 50 nm between cycles 1 and 3, with little change thereafter. The surface fractal dimension of these blobs is 1.9 for cycle 1 gels and fairly uniform at ~ 2.1 for cycles 3 and 6 gels. A fractal dimension less than 2 indicates that the surface is diffuse. This suggests that there is a significant amount of loosely bound polymer available at the surfaces of the blobs to reinforce the gel structure during later thermal cycles. It is noteworthy that the gel correlation length ξ_{fixed} and blob size R are similar to the principal length scales of the gel phase described in a previous study,[5] although determined from a different model. Our interpretation is that the gel phase consists of polymer crystallites of size no more than a few nanometers surrounded by uncrystallized polymer. As is usual in polymer crystallization, significant portions of chains participating in crystallization are expected to extend from the crystallite surfaces. These may extend to other crystallites or be entangled with chains extending from other crystallites, creating a gel. We note that the natural length scales of our PVA stock—a radius of gyration of 32–38 nm, as determined from a simple self-avoiding random-walk model,[16] and contour length of 830–1060 nm based on its molecular weight—is consistent with gel length scales measured here.

The maximum size of the mass fractal aggregates is at or above the largest length scale probed by the USANS data, limiting our ability to determine the large-scale structure accurately. However, it is clear from the data of Fig. 4 that the maximum length scale increases abruptly between cycles 1 and 3, but likely does not change much between cycles 3 and 6.

The hierarchy of structures described above is corroborated by direct imaging. The AFM images shown in Fig. 9 reveal structures on several scales. At the smallest scales imaged, seen in Fig. 9(a), dense regions with sizes ~ 100 nm are seen surrounding randomly distributed regions with sizes from several 100 nm to ~ 1 μm. Although the softness of the gel limits the resolution of the images so that no structure can be seen inside the denser regions, the pictures are consistent with the model of connected polymer blobs forming an aggregate around polymer-poor pores. At larger scales, Fig. 9(b), it is seen that the dense regions form structures of at least a few micrometers. It is only at very large scales, as in Fig. 9(c), that a more uniform structure exists, though even then ridges and furrows, which may be relics of dendritic ice crystals, are evident.

We note that structures similar to those shown by our AFM imaging have been demonstrated by Fergg et al.[30] using confocal microscopy, although in that case the pores were considerably larger (~ 6 μm), perhaps due to the limited ability of optical techniques to resolve smaller details in such a complicated material.

Previous mechanical studies[1,2,4,31] show that Young's modulus of PVA hydrogels increases monotonically with the number of thermal cycles. This increase could result from both the increased crystallinity indicated by the decrease in the gel length scale ξ_{fixed} and exponent b, and the increased size of the largest gel aggregates, as shown by the USANS data. However, the observation that the main change in the large structure occurs between cycles 1 and 3 while the mechanical strength continues to increase at least up to cycle 6 suggests that the increase is mainly due to strengthening of the gel phase within the blob structures.

B. Anisotropic gels

Anisotropic gels—i.e., those subjected to a strain during thermal cycling—show clear differences in scattering between the directions parallel and perpendicular to the strain direction, thus producing the elliptical patterns in the two-dimensional SANS data shown in Fig. 1. Figure 5 shows the differential scattering cross sections determined by SANS and USANS for the two principal directions measured for a sample subjected to a strain of 75% after one thermal cycle and cycled an additional five times (the corresponding isotropic scattering from Fig. 4 is shown for comparison).

It is immediately evident that the most striking differences between scattering from isotropic and anisotropic samples are seen at low q. This is quantified by the fits of combined SANS/USANS data to the functional form of Eq. (8), which show that while the size of the fractal aggregates in the direction perpendicular to the processing strain remains somewhat constant at a few micrometers, the aggregates are consistently larger than the maximum size that can be probed by USANS in the parallel direction (see Table III). The blob sizes determined from the combined data sets also show a markedly larger value in the direction parallel to the processing strain. We note, however, that this increase is certainly less than the strain itself, suggesting some relaxation during the remaining cycles. Together, these observations suggest that, while the blobs are elongated along the strain direction (and possibly slightly contracted in the perpendicu-

lar direction), the main source of the permanent anisotropic mechanical properties is at the largest length scales, as has been suggested previously.[5]

In order for the structural rearrangements that take place upon stretching to become permanent after further cycling, additional cross-links must form to prevent the structure from collapsing back to an isotropic state after the strain is released. To study anisotropy at small length scales, we acquired SANS data for samples having applied strains from 0 (isotropic) to 0.75 in increments of 0.25. For each of the small length-scale parameters—gel length scale, gel exponent, blob size, and blob surface fractal dimension—we performed linear fits versus strain to determine whether there was a significant trend.

Figure 6 shows no significant change in the surface fractal dimension between cycles 3 and 6 for isotropic gels. However, there is a significant trend versus the processing strain in the parallel direction of the anisotropic samples. In this direction, p-values of 0.032 and 0.035 for cycles 3 and 6, respectively, indicate that the observed trend is less than 4% likely to have occurred by chance. No significant trend is seen in the perpendicular direction, so these data are fit to constant values (horizontal lines in Fig. 6), resulting in very nearly the same values for cycles 3 and 6.

No systematic dependence on the processing strain is evident in Fig. 7, showing that the gel phase itself does not exhibit significant anisotropy. However, Fig. 8 shows that the gel exponent increases slightly between cycles 3 and 6. There may be slight dependence on the processing strain for the parallel direction as one linear trend was significant at the 5% level, but not the perpendicular direction: the p-values are 0.041 and 0.13 in the parallel direction and 0.61 and 0.18 in the perpendicular direction, for cycles 3 and 6, respectively.

The relatively minor change in gel length scale and exponent as a function of processing strain argues that rearrangements at this scale are unimportant to the anisotropy in mechanical properties that has been previously reported.[4] We hypothesize that the dense polymer network inside the blobs is much stronger than the bulk gel so that when strain is applied it is easier to change the position of blobs in the gel than to stretch the blobs themselves. This would cause a net alignment of connections between blobs in the direction of strain, increasing the roughness of blob surfaces, and hence the associated fractal dimension, in that direction. It is interesting that the mechanical data show no significant dependence on processing strain of Young's modulus in the perpendicular direction, in agreement with the lack of structural change in that direction seen here.

V. CONCLUSION

By applying a stress during thermal processing, anisotropic PVA hydrogels can be produced. Previous results have shown that with proper selection of processing parameters, the bulk anisotropic elastic properties can be made to closely match those of cardiovascular tissue, making the material suitable for the manufacture of grafts and other cardiovascular prostheses. However an understanding of the structural features resulting in this anisotropy is important.

We performed SANS and USANS to study anisotropic hydrogels at length scales from 2 nm to 10 μm, extending our previous neutron scattering work[5] to larger length scales. We modeled the structure as blobs of size $\sim$50 nm arranged in an aggregate with mass fractal characteristics up to a maximum length scale of several micrometers. The polymer inside the blobs was described by a Horkay–Geissler stretched-exponential correlation function. Systematically varying the number of thermal cycles revealed that the resulting increase in gel strength at macroscopic scales is due to an increase in aggregate size, especially for early cycles, as well as an increase in strength of the gel phase, perhaps due to increased crystallinity. It is also evident that mechanical anisotropy resulting from strain applied during processing is due to stretching of the mass fractal aggregates and alignment of the aggregate building blocks. The building blocks themselves are slightly elongated in the direction parallel to the applied processing strain, but little or no anisotropy is observed in the polymer arrangement at the smallest scales.

[1] C. M. Hassan and N. A. Peppas, Adv. Polym. Sci. **153**, 37 (2000).
[2] W. K. Wan, G. Campbell, Z. F. Zhang, A. J. Hui, and D. R. Boughner, J. Biomed. Mater. Res. **63**, 854 (2002).
[3] G. Paradossi, F. Cavalieri, E. Chiessi, C. Spagnoli, and M. K. Cowman, J. Mater. Sci.: Mater. Med. **14**, 687 (2003).
[4] L. E. Millon, H. Mohammadi, and W. K. Wan, J. Biomed. Mater. Res. **79**, 305 (2006).
[5] L. E. Millon, M.-P. Nieh, J. L. Hutter, and W. Wan, Macromolecules **40**, 3655 (2007).
[6] H. Haruguchi and S. Teraoka, J. Artif. Organs **6**, 227 (2003).
[7] S. T. Rashid, H. J. Salacinski, B. J. Fuller, G. Hamilton, and A. M. Seifalian, Cell Proliferat. **37**, 351 (2004).
[8] N. A. Peppas, Makromol. Chem. **176**, 3433 (1975).
[9] Y. Mori, H. Tokura, and M. Yoshikawa, J. Mater. Sci. **32**, 491 (1997).
[10] P. J. Willcox, J. D. W. Howie, K. Schmidt-Rohr, D. A. Hoagland, S. P. Gido, S. Pudjijanto, L. W. Kleiner, and S. Ventatraman, J. Polym. Sci. Pol. Phys. **37**, 3438 (1999).
[11] C. J. Glinka, J. G. Barker, B. Hammouda, S. Krueger, J. J. Moyer, and W. J. Orts, J. Appl. Crystallogr. **31**, 430 (1998).
[12] D. F. R. Mildner, B. Hammouda, and S. R. Kline, J. Appl. Crystallogr. **38**, 979 (2005).
[13] J. G. Barker, C. J. Glinka, J. J. Moyer, M. H. Kim, A. R. Drews, and M. Agamalian, J. Appl. Crystallogr. **38**, 1004 (2005).

[14] S. R. Kline, J. Appl. Crystallogr. **39**, 895 (2006).

[15] J. A. Lake, Acta Crystallogr. **23**, 191 (1967).

[16] P.-G. de Gennes, *Scaling Concepts in Polymer Physics* (Cornell University Press, Ithaca, NY, 1979).

[17] R. Ricciardi, G. Mangiapia, F. Lo Celso, L. Paduano, R. Triolo, F. Auriemma, C. De Rosa, and F. Lauprêtre, Chem. Mater. **17**, 1183 (2005).

[18] F. Auriemma, C. De Rosa, and R. Triolo, Macromolecules **39**, 9429 (2006).

[19] S. Mallam, A.-M. Hecht, and E. Geissler, J. Chem. Phys. **91**, 6447 (1989).

[20] E. Geissler, F. Horkay, and A.-M. Hecht, Macromolecules **24**, 6006 (1991).

[21] F. Horkay, A.-M. Hecht, S. Mallam, E. Geissler, and A. R. Rennie, Macromolecules **24**, 2896 (1991).

[22] E. Geissler, F. Horkay, and A.-H. Hecht, Phys. Rev. Lett. **71**, 645 (1993).

[23] F. Horkay, A.-M. Hecht, and E. Geissler, Macromolecules **27**, 1795 (1994).

[24] S. Mallam, F. Horkay, A.-M. Hecht, A. R. Rennie, and E. Geissler, Macromolecules **24**, 543 (1991).

[25] P. Debye, H. R. Anderson, Jr., and H. Brumberger, J. Appl. Phys. **28**, 679 (1957).

[26] A. Emmerling, R. Petricevic, A. Beck, P. Wang, H. Scheller, and J. Fricke, J. Non-Cryst. Solids **185**, 240 (1995).

[27] M. Shibayama, H. Kurokawa, S. Nomura, M. Muthukumar, R. S. Stein, and S. Roy, Polymer **33**, 2883 (1992).

[28] S.-H. Chen and J. Teixeira, Phys. Rev. Lett. **57**, 2583 (1986).

[29] R. Ricciardi, F. Auriemma, C. De Rosa, and F. Lauprêtre, Macromolecules **37**, 1921 (2004).

[30] F. Fergg, F. J. Keil, and H. Quader, Colloid Polym. Sci. **279**, 61 (2001).

[31] F. Yokoyama, I. Masada, K. Shimamura, T. Ikawa, and K. Monobe, Colloid Polym. Sci. **264**, 595 (1986).